Phosphate Adsorption Properties of Magnetite-Based Nanoparticles

T. J. Daou,*,† S. Begin-Colin,*,† J. M. Grenèche,‡ F. Thomas,§ A. Derory,† P. Bernhardt,|| P. Legaré,|| and G. Pourroy†

Institut de Physique et Chimie des Matériaux de Strasbourg, UMR CNRS-ULP 7504, 23, rue du Loess, BP 43, 67034 Strasbourg cedex 2, France, Laboratoire de Physique de L'Etat Condensé, UMR CNRS 6087, Université du Maine, 72085, Le Mans, cedex 9, France, Laboratoire Environnement et Minéralurgie, UMR 7569 CNRS INPL, 54501 Vandoeuvre-Lès-Nancy, and Laboratoire des Matériaux, Surfaces et Procédés pour la Catalyse (LMSPC), UMR 7515, CNRS-ECPM, Université Louis Pasteur, 25 rue Becquerel, 67087, Strasbourg cedex 2, France

Received April 17, 2007. Revised Manuscript Received June 25, 2007

Magnetite nanoparticles of 40 nm in size have been phosphated in orthophosphoric acid. Large phosphatation rates, equivalent to goethite capacity, have been pointed out, and the possibility of phosphatation−dephosphatation cycles has been proved. Phosphatation occurs rapidly, inhibits the dissolution of magnetite and does not modify the structure and the magnetization of magnetite. IR spectroscopy, X-ray photoelectron spectroscopy (XPS) analysis, and Mössbauer spectrometry have shown that phosphatation occurs by interaction with both positively charged groups and hydroxyl sites at the surface of magnetite and more precisely with Fe^{3+} in octahedral sites. The main surface species would be a protonated binuclear species and the top layer would be in the (111) plane. The chemical stability of magnetite during cycling and its magnetic macroscopic moment allowing an easy recycling are promising for technological uses.

1. Introduction

The strong affinity of phosphorus-based ions toward metals or metal (hydr)oxides is widely exploited in numerous industrial applications. The most widespread process is phosphating of metal surfaces, which ensures protection of ferrous or nonferrous metallic materials against oxidative corrosion. In the water treatment industry, adsorption of phosphate by metal (hydr)oxides, mainly iron hydroxides, has proven to be an effective method for removing phosphorus from wastewater.[1−17] Among the numerous works devoted to this topic, most deal with adsorption on goethite (α-FeOOH). Goethite is a stable crystalline iron oxyhydroxide, commonly encountered in nature and easy to synthesize in the laboratory, and therefore, it is very often used as a model solid for adsorption studies.

As far as magnetic iron oxides are concerned, most studies on the interaction between phosphate and oxides deal with the effect of phosphating on the magnetic properties of superparamagnetic maghemite (γ-Fe_2O_3) nanoparticles and on the coupling interaction between magnetic nanoparticles.[18−23] Magnetite (Fe_3O_4) was the object of far less numerous investigations of that type. For example, the magnetite surface was used as nucleus for heterogeneous Ca-phosphate precipitation.[24] But to our knowledge, there was up to now no published investigation devoted to phosphating of magnetite and to its potential as a phosphate adsorbent.

Different phosphorus-based ions were studied as possible adsorbents. Phosphonic acid-based molecules are more and more involved for SAMs (self-assembled monolayers) formation deposited on metallic and metal oxide surfaces. SAMs are used as protective films to passivate metal

* Corresponding author. Fax: (+33) 3.88.10.72.47. Tel.: (+33) 3.88.10.71.92. E-mail: daou@ipcms.u-strasbg.fr (T.J.D.); begin@ipcms.u-strasbg.fr (S.B.-C.).
† Institut de Physique et Chimie des Matériaux de Strasbourg.
‡ Université du Maine.
§ Laboratoire Environnement et Minéralurgie.
|| Université Louis Pasteur.

(1) Benjamin, M. M. *Water Chemistry*; McGraw−Hill Higher Education: Singapore, 2002.
(2) Yeoman, S.; Stephenson, T.; Lester, J. N.; Perry, R. *Environ. Pollut.* **1988**, *49*, 183.
(3) Chen, Y. S. R.; Butler, J. N.; Stumm, W. *Environ. Sci. Technol.* **1973**, *7*, 327.
(4) Lijklema, L. *Environ. Sci. Technol.* **1980**, *14*, 537.
(5) Arai, Y.; Sparks, D. L. *J. Colloid Interface Sci.* **2001**, *241*, 317.
(6) Laitti, E.; Persson, P.; Öhman, L. O. *Langmuir* **1998**, *14*, 825.
(7) Durif, A. *Crystal Chemistry of Condensed Phosphates*; Plenum: New York, 1995.
(8) Laitti, E.; Persson, P.; Öhman, L. O. *Langmuir* **1996**, *12*, 2969.
(9) Connor, P. A.; McQuillan, A. J. *Langmuir* **1999**, 2916.
(10) Yee, C.; Kataby, G.; Ulman, A.; Prozorov, T.; White, H.; King, A.; Rafailovich, M.; Sokolov, J.; Gedanken, A. *Langmuir* **1999**, *15*, 7111.
(11) Antelo, J.; Avena, M.; Fiol, S.; Lopez, R.; Arce, F. *J. Colloid Interface Sci.* **2005**, *285*, 476.
(12) Chitrakar, R.; Tezuka, S.; Sonoda, A.; Sakane, K.; Ooi, K.; Hirotsu, T. *J. Colloid Interface Sci.* **2006**, *298*, 602.
(13) Luengo, C.; Brigante, M.; Antelo, J.; Avena, M. *J. Colloid Interface Sci.* **2006**, *300*, 511.
(14) Nowack, B.; Stone, A. T. *Water Res.* **2006**, *40*, 2201.
(15) Randon, J.; Blanc, P.; Paterson, R. *J. Membr. Sci.* **1995**, *98*, 119.
(16) Borggaard, O. K.; Raben-Lange, B.; Gimsing, A. L.; Strobel, B. W. *Geoderma* **2005**, *127*, 270.
(17) Zeng, L.; Li, X.; Liu, J. *Water Res.* **2004**, *38*, 1318.
(18) Tronc, E.; Prené, P.; Jolivet, J. P.; Dormann, J. L.; Grenèche, J. M. *Hyperfine Interact.* **1998**, *112*, 97.
(19) Brice-Profeta, S.; Arrio, M.-A.; Tronc, E.; Menguy, N.; Letard, I.; Cartier dit Moulin, C.; Noguès, M.; Chanéac, C.; Jolivet, J.-P. Sainctavit, Ph. *J. Magn. Magn. Mater.* **2005**, *228*, 354.
(20) Tronc, E.; Ezzir, A.; Cherkaoui, R.; Chanéac, C.; Noguès, M.; Kachkachi, H.; Fiorani, D.; Testa, A. M.; Grenèche, J. M.; Jolivet, J. P. *J. Magn. Magn. Mater.* **2000**, *221*, 63.
(21) Prodan, D.; Chanéac, C.; Tronc, E.; Jolivet, J. P.; Cherkaour, R.; Ezzir, A.; Noguès, M.; Dormann, J. L. *J. Magn. Magn. Mater.* **1999**, *203*, 63.
(22) Jolivet, J. P.; Chanéac, C.; Tronc, E. *Chem. Commun.* **2004**, 481.
(23) Tronc, E.; Jolivet, J. P. *Hyperfine Interact.* **1986**, *28*, 525.
(24) Karapinar, N.; Hoffmann, E.; Hahn, H. H. *Water Res.* **2006**, *40*, 1210.

10.1021/cm071046v CCC: $37.00
Published on Web 08/14/2007

surfaces, interface corrosion protectors, adhesion promoters, or for biomedical applications such as protein adsorption, cell behavior, or fabrication of tailored sensor surfaces.[25−37] The phosphonate group is used as a coupling agent for covalent and high-coverage grafting of organic molecules at interfaces.

In all the aforementioned adsorption or grafting studies, the key factor is the structure of the complex formed between the phosph(on)ate group and the surface sites of the solid. It is generally agreed that phosphate adsorbed on goethite forms inner-sphere complexes where one or two oxygen atoms of phosphate anions bind directly one or two iron atoms at the interface respectively.[11,12,38] However, the fine mechanism of phosphate interaction with the iron (hydr)oxide interface is still not established. There is indeed some consensus about the dominance of the binuclear bond, but the mono-, bi-. or trinuclear nature of the complexes is still a matter of debate. Another often discussed parameter is the degree of protonation of mono- and binuclear phosphate complexes. Unfortunately, infrared spectroscopy and NMR studies did not yet succeed in establishing unambiguous peak assignments for phosphate.[14] Therefore, further refinement of knowledge on the bonding of phosphorus molecules on iron (hydr)oxides requires the use of several characterization techniques.

The present study is an investigation of the mechanisms governing the adsorption of orthophosphate on magnetite nanoparticles. The purposes were to determine the type of bonding, the effect of phosphating on the properties of magnetite, and to evaluate the potential application of magnetite for phosphorus removal in water treatment. To this end, magnetite nanoparticles with an average grain size of 40 nm have been phosphated and a multitechnique approach, including potentiometric titration, electrokinetic measurements, X-ray diffraction, Mössbauer, X-ray photoelectron spectroscopy (XPS) and infrared spectroscopies, scanning electron microscopy, and ZFC/FC measurements, was followed.

2. Experimental Section

2.1. Synthesis of Magnetite Nanoparticles. Magnetite nanoparticles were prepared in two steps. First coprecipitation of ferrous Fe^{2+} and ferric Fe^{3+} ions by a $(N(CH_3)_4OH)$ solution at 70 °C was achieved. After this step, the average particle size was 12 ± 2 nm and the specific surface area was 117 m^2/g. The second step was hydrothermal treatment at 250 °C.[39] The final composition of magnetite was $Fe_{2.95}O_4$, the average particle size was 39 ± 5 nm, and the specific surface area was 31 m^2/g. The magnetite nanoparticles were demonstrated to exhibit the (111) face.[39]

2.2. Phosphating of Magnetite Nanoparticles. An amount of 50 mg of the magnetite nanoparticles was dispersed in 50 mL of deionized water in a 100 mL flask, using an ultrasonic bath. Different amounts of orthophosphoric acid (85%) were added to the suspension. The adsorption reaction was carried out for 24 h at room temperature under argon stream, with mechanical stirring. The reaction pH was initially fixed at 3 by adding HCl or NaOH so that the dominant phosphate species was $H_2PO_4^-$. During the reaction, the pH stayed close to 3.

To determine the amount of phosphate molecules grafted at the surface of magnetite, the phosphated nanoparticles were magnetically separated from solution and the solution was recuperated. The phosphated nanoparticles were then washed three times with distilled water and then one time with absolute ethanol and dried in vacuum at room temperature for 12 h. The washing procedure ensured that hydrogen-bonded phosphate multilayers are removed from the surface. The amount of phosphate eliminated in the washing solutions was analyzed following the molybdenum blue heretopolyphosphate complex method, with $(NH_4)_6Mo_7O_{24}\cdot 4H_2O$ as the molybdate reagent.[40] The amount of grafted phosphate was deduced in order to draw adsorption isotherms of phosphate on magnetite. The phosphorus to iron ratio was confirmed by inductively coupled plasma atomic emission spectroscopy (ICP-AES) analysis.

Tests of desorption of phosphate grafted on magnetite were achieved by dispersing the phosphated particles in a 1 M NaOH solution for 24 h, and the amount of desorbed phosphate was analyzed according to the above method.

Structural characterization was performed on phosphated magnetite nanoparticles with the following phosphatation rates (amount of grafted phosphate in milligrams per gram of magnetite nanoparticles): 2.06, 3.9, and 5.2 P-mg/g named, respectively, P1, P2, and P3.

2.3. Characterization Techniques. The surface charge of magnetite was measured by potentiometric titration on a Radiometer titration chain including an Ionometer−pHmeter (PHM250), an autoburette (ABU901), and a thermostatic titration cell (HMT200) regulated at 25 ± 0.1 °C. The pH was measured with a GK2401 (Radiometer) combination electrode, and the titration cell was kept under nitrogen stream.

The identification of crystalline phases in the synthesized particles was performed using a Siemens D-500 X-ray diffractometer with high-intensity Co Kα radiation (25 mA, 35 kV, $\lambda = 1.789$ A). The lattice parameter calculations were obtained with the UFIT software. The average crystallite size was estimated following the Scherrer equation.

Infrared spectra were recorded with a Fourier transform infrared (FTIR) spectrometer (Digilab FTS 3000). Samples were gently ground and diluted in nonabsorbent KBr matrixes.

^{57}Fe Mössbauer spectra were recorded at 300 K and at 77 K on a conventional constant acceleration transmission spectrometer with

(25) Guerero, G.; Mutin, P. H.; Vioux, A. *Chem. Mater.* **2001**, *13*, 4367.
(26) Frantz, R.; Durand, J. O.; Granier, M.; Lanneau, G. F. *Tetrahedron Lett.* **2004**, *45*, 2935.
(27) Mutin, P. H.; Lafond, V. A.; Popa, F.; Granier, M.; Markey, L.; Dereux, A. *Chem. Mater.* **2004**, *16*, 5670.
(28) Mutin, P. H.; Guerrero, G.; Vioux, A. *J. Mater. Chem.* **2005**, *15*, 3761.
(29) Textor, M.; Ruiz, L.; Hofer, R.; Rossi, A.; Feldman, K.; Haehner, G.; Spencer, N. D. *Langmuir* **2000**, *16*, 3257.
(30) Frantz, R.; Granier, M.; Durand, J. O.; Lanneau, G. F. *Tetrahedron Lett.* **2002**, *43*, 9115.
(31) Kar, S.; Durand, J. O.; Granier, M.; Joly, P.; Melnyk, O. *Tetrahedron Lett.* **2003**, *44*, 5617.
(32) Gao, W.; Dickinson, L.; Morin, C. F. G.; Reven, L. *Langmuir* **1996**, *12*, 6429.
(33) Tosatti, S.; Michel, R.; Textor, M.; Spencer, N. D. *Langmuir* **2002**, *18*, 3537.
(34) Hofer, R.; Textor, M.; Spencer, N. D. *Langmuir* **2001**, *17*, 4014.
(35) Textor, M.; Ruiz, L.; Hofer, R.; Rossi, A.; Feldman, K.; Hähner, G.; Spencer, N. D. *Langmuir* **2000**, *16*, 3257.
(36) Tourtin, F.; Armand, P.; Ibanez, A.; Tourillon, G.; Philippot, E. *Thin Solid Films.* **1998**, *322*, 85.
(37) Sahoo, Y.; Pizem, H.; Fried, T.; Golodnitsky, D.; Burstein, L.; Sukenik, C. N.; Markovich, G. *Langmuir* **2001**, *17*, 7907.
(38) Li, L.; Stanforth, R. *J. Colloid Interface Sci.* **2000**, *230*, 12.
(39) Daou, T. J.; Pourroy, G.; Bégin, S.; Grenèche, J. M.; Ulhaq-Bouillet, C.; Legaré, P.; Bernhardt, P.; Leuvrey, C.; Rogez, G. *Chem. Mater.* **2006**, *18*, 4399.
(40) Todd, J. C.; Stanford, A. H. *Clinical Diagnosis by Laboratory Methods*; W. B. Saunders Co.: Philadelphia, 1940; Vol. 9.

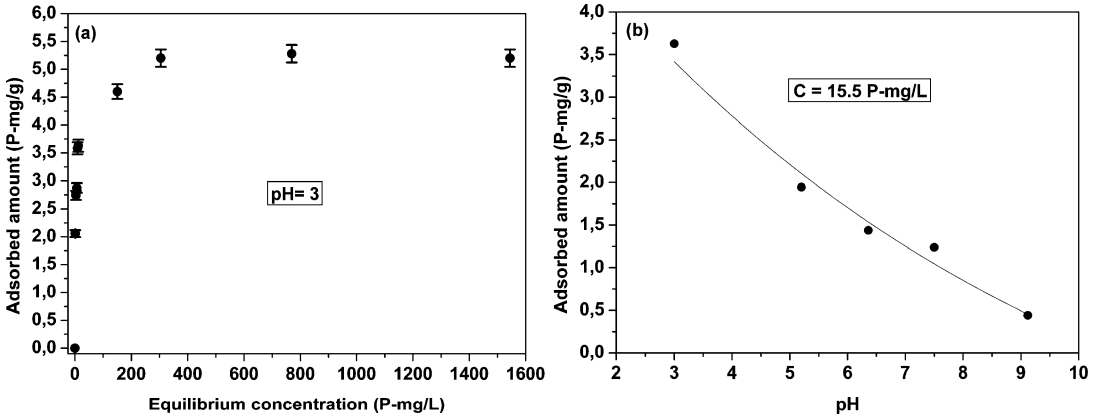

Figure 1. Adsorption isotherm of phosphate at the surface of magnetite nanoparticles at pH = 3 (a) and maximal adsorption of phosphate from a solution with 15.5 P-mg/L as a function of pH (b).

a ^{57}Co(Rh) source and a bath cryostat. An α-Fe foil was used as a calibration sample. The spectra were fitted by means of the MOSFIT program,[41] and an α-Fe foil was used as a calibration sample. The values of isomer shift are quoted to that of α-Fe at 300 K.

X-ray photoelectron spectroscopy (XPS) was performed with a ThermoVGScientific photoelectron spectrometer equipped with a twin anode providing both unchromatized Al Kα and Mg Kα radiations (1486.6 and 1453.6 eV, respectively). The spectrometer equipped with a multichannel detector operated in the constant resolution mode with a pass energy of 20 eV. The total resolution of the system was estimated at 0.55 eV. Spectra were referenced to the aliphatic hydrocarbon C1s signal at 285 eV.

The microstructure of the particles was studied by scanning electron microscopy (SEM) (JEOL 6700F) and transmission electron microscopy (TEM) and high-resolution TEM (HRTEM) with a TOPCON model 002B transmission electron microscope, operating at 200 kV, with a point to point resolution of 0.18 nm.

The electrophoretic mobility of the particles was measured with a Malvern Zetasizer (NanoZS) as a function of pH in 10^{-3} M $NaClO_4$ solution. The zeta potential was calculated from the electrophoretic mobility after the Hückel law which takes into account the fact that the radius of the particles is small by comparison with the thickness of the electric double layer.

ZFC/FC measurements were performed using a superconducting quantum interference device (SQUID) magnetometer (Quantum Design MPMS-XL model) between 4 and 400 K under a magnetic field of 10 Oe. Hysteresis cycles were recorded at room temperature by using a vibrating sample magnetometer.

3. Results and Discussion

3.1. Phosphate Adsorption. *(a) Quantitative Aspects.* The adsorption isotherm of phosphate on the surface of 40 nm magnetite nanoparticles at pH = 3 versus the equilibrium orthophosphoric acid concentration appears in Figure 1. At this pH, the magnetite surface is positively charged as observed on the zeta potential curve as a function of pH of magnetite nanoparticle given in Figure 2. It exerts electrostatic attraction toward the monovalent phosphate. Possible dissolution of the magnetite in the adsorption conditions was checked by analyzing the solution for iron after 3 days of contact. Only 0.02% of the iron was dissolved, proving that

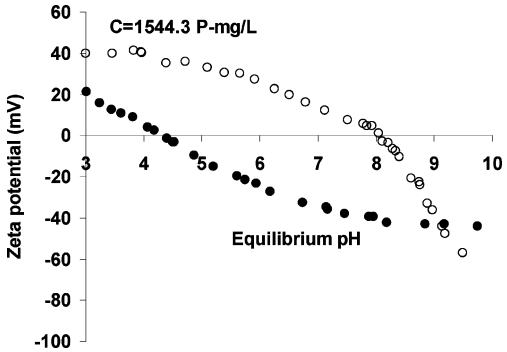

Figure 2. Zeta potential measurements as a function of pH of magnetite nanoparticles before (open circle) and after phosphatation (P3 sample; solid circle) in 10^{-3} M $NaClO_4$.

phosphating, as expected, inhibits the dissolution of magnetite.

For equilibrium phosphate concentrations above 300 P-mg/L a maximum adsorbed amount of 5.2 P-mg/g is reached, in other words 0.168 mmol/g, 5.4 μmol/m^2, 3.26 molecules/nm^2, or 3.26×10^{14} molecules/cm^2 (Figure 1a). This maximum is ensured by the elimination of excess phosphate during washing treatments. Therefore, we do not observe a linear increase at high P concentrations such as that described by Li et al.,[38] suggesting that in our case a phosphate monolayer does cover the magnetite surface.

The amounts of phosphate adsorbed from a 15.5 P-mg/L solution (Figure 1b) decreased with increasing pH, as already described for similar experiments on goethite,[11,12,38] on iron oxide tailings (mainly magnetite and goethite with impurities)[17] and on ferrihydrite.[5] This is mainly explained by the surface charge of magnetite deduced from the zeta potential curve of magnetite as a function of pH (Figure 2). The isoelectric point (IEP) of magnetite is located at pH = 8 (Figure 2) in agreement with the point of zero charge (PZC) pH_{PZC} = 7.9 determined by titration and with values given in literature for magnetite (Table 1).[42−45] When the pH is increased, the surface charge of magnetite varies from

(41) Teillet, J.; Varret, F. unpublished MOSFIT program, Université du Maine: Le Mans, France.

(42) Sun, Z.-X.; Su, F.-W.; Forsling, W.; Samskog, P.-O. *J. Colloid Interface Sci.* **1998**, *197*, 151.
(43) Illès, E.; Tombacz, E. *Coll. Surf. A* **2004**, *230*, 99.
(44) Marmier, N.; Delisée, A.; Fromage, F. *J. Colloid Interface Sci.* **1999**, *211*, 54.
(45) Catalette, H.; Dumonceau, J.; Ollar, P. *J. Contam. Hydrol.* **1998**, *35*, 151.

Table 1. Surface Sites Density and pH_{PZC} and IEP Values Reported for Magnetite Particles

ref	purity (%)	specific surface (m^2/g)	surface sites density (sites/nm^2)	pH_{PZC}	IEP
45	96	18.3	4.4	5.55 (silica impurities)	
44	99.99	1.8	1.14 mol/L for 1 g:1.9	6.3	
43	99.9	95.3	1.6	7.9	8
42	99.9	95.2	5.2		6
our study	99.9	31	2.2	7.9	8

positive to negative, according to the point of zero charge due to deprotonation of surface hydroxyls. At the same time, the species in solution change from mono- to di- and tribasic. Therefore, adsorption is progressively shielded by electrostatic repulsions between the increasingly negative surface charge and the increasingly multivalent anions in solution.

The phosphate adsorption capacity observed on magnetite nanoparticles is similar to that obtained with goethite,[11,12,16,38] ferrihydrite,[5,16] $Al(OH)_3$,[16] iron oxide tailings (30% iron oxide),[17] and hematite at similar pH.[17,46] The highest adsorption is reported for akaganeite (59.6 P-mg/g)[47] due to its tunnel structure. Nevertheless, the reported values for phosphate adsorption capacity are often given in milligrams of P per gram or micromoles per gram, but the most pertinent values should be those taking into account the specific surface. Therefore, the phosphate adsorption capacity of these magnetite nanoparticles may be considered as equivalent to, even higher than, that of the other tested adsorbents.

The applicability of magnetite nanoparticles as an adsorbent depends not only on the adsorption capacity but also on its reusability. Phosphate desorption was studied on a 4.6 P-mg/g phosphated magnetite in 1 M NaOH solution as an eluant. 90% of phosphate was removed. The reloaded amount decreased slightly after the first loading and seemed then to stabilize around 3.5 P-mg/g (Figure 3). XRD measurements showed that further desorption/adsorption cycles do not modify the magnetite structure. Similar experiments on goethite have demonstrated the poor potential reusability of goethite (13−14%) for adsorbed phosphate by comparison with akaganeite (β-FeOOH) (67%).[12] This low desorbability capacity of goethite was also confirmed by Zeng et al.[17] So, although nanocrystallized magnetite is less promising than microporous akaganeite (β-FeOOH)[12] in terms of absorbed amounts, it is an interesting phosphate adsorbent because of its adsorbed amounts, similar to those of the reference phosphate adsorbent, goethite, its chemical stability during cycles, and its magnetic macroscopic moment allowing easy recycling.

(b) Phosphatation Rate and Surface Site Density. Phosphate adsorption is generally thought to occur either by electrostatic interaction of phosphate anions with $Fe-OH_2^+$ sites or by ligand exchange, a phosphate oxygen replacing an hydroxyl oxygen on the surface.[11,12,38] From the maximum amount of phosphate grafted at the surface of magnetite, the accumulation of phosphate is then one phosphate molecule

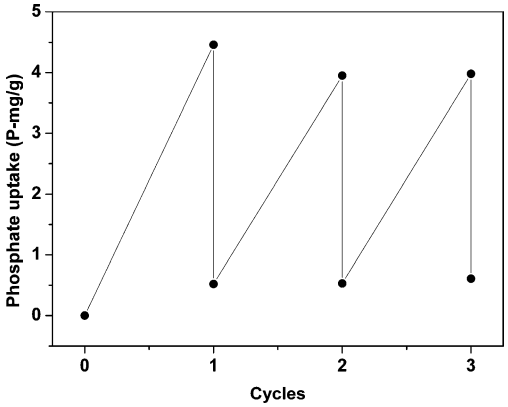

Figure 3. Adsorption/desorption cycles of phosphate on the surface of magnetite nanoparticles from a solution with 155 P-mg/L.

per 0.31 nm^2, the area of the phosphate molecule being 0.24 nm^2. It leads to a surface coverage of about 78% and the presence of ~3.3 phosphate molecules per squared nanometer of magnetite. This value must be compared to the density of active proton binding sites at the surface of magnetite nanoparticles. As all oxides, magnetite is an amphoteric solid, which develops charges in the protonation and deprotonation reactions of Fe−OH sites on the surface. However, all Fe−OH sites are not equivalent and less than 20% of the surface sites are generally considered to be ionizable. The amount of active proton binding sites can be evaluated from acid−base titrations at different ionic strengths. The density of protonable sites measured by titration is 2.2 ± 0.2 sites/nm^2. This value falls within the reported values given in Table 1, which are rather scattered. Similar discrepancies have also been observed in the case of goethite, 3.45 (see ref 11) or 1.7 sites/nm^2 (see ref 14), and may be related to the purity of products. Indeed magnetite with silica impurities displays higher surface site density. In our case, it is in the same range as that determined for magnetite with the same purity and the same IEP and PZC.[43]

The measured active proton binding site density is lower than the number of phosphate molecules adsorbed at the surface of magnetite. That means that whatever the type of bonding, i.e., mono, bi, or trinuclear, phosphatation occurs also via interaction with nonionizable OH sites. Moreover, the zeta potential at pH = 3 after phosphatation is lower than before phosphatation showing that the surface is less positive (Figure 2). Indeed, the zeta potential curve shifts toward acidic pH after phosphatation proving the success of the phosphatation of the magnetite nanoparticles.[11,38] At pH = 3, the zeta potential value of phosphated magnetite is around 20 mV. Phosphate lowers the surface charge by replacing the less acidic iron hydroxyl groups with the much more acidic phosphate hydroxyl groups, but the phosphated surface is always positively charged, showing that all $Fe-OH_2^+$ sites have not been involved in phosphate complexes. Thus, in our experimental conditions, it may be advanced that phosphates under the form of $H_2PO_4^-$ species at pH = 3 interact with both positively charged groups and hydroxyl sites at the surface of magnetite to form phosphate complexes.[25,48,49] Further investigations, detailed below, have been conducted to investigate the type of phosphate complexes at the surface of magnetite.

(46) Nooney, M. G.; Murrell, T. S.; Corneille, J. S.; Rusert, E. I.; Rossner, L. R.; Goodman, D. W. *J. Vac. Sci. Technol. A* **1996**, *14*, 1357.
(47) Deliyanni, E. A.; Peleka, E. N.; Lazaridis, N. K. *Sep. Purif. Technol.* **2007**, *52*, 478.

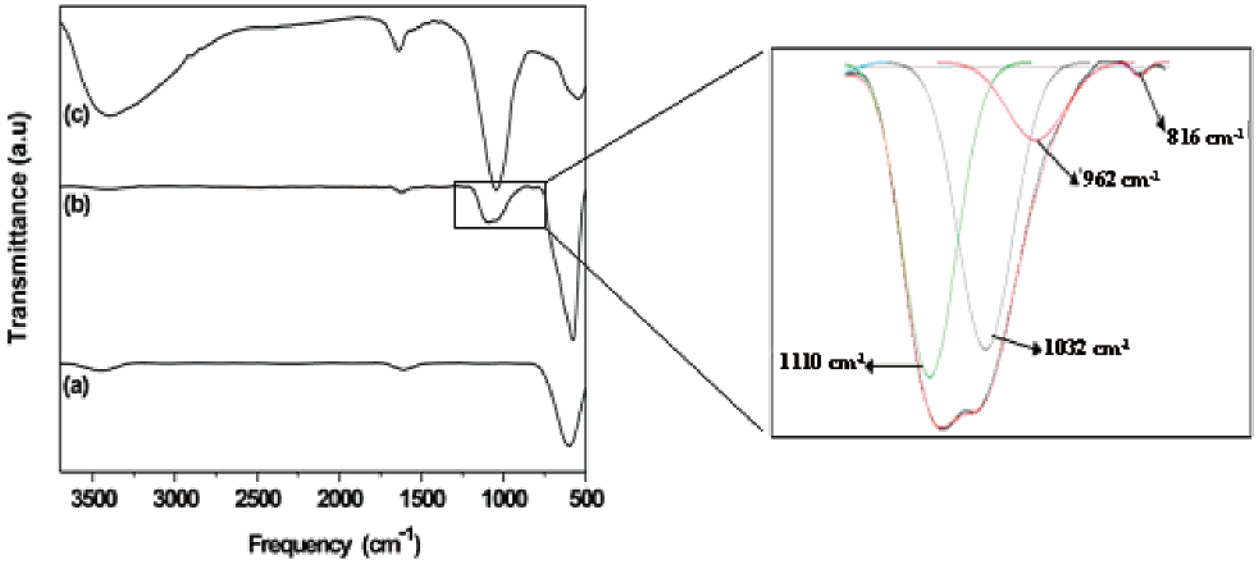

Figure 4. FTIR spectra of magnetite before (a) and after phosphatation (P3 sample) (b), commercial $FePO_4$ (c), and deconvoluted spectrum of phosphated bands.

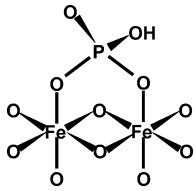

Figure 5. Scheme of phosphate and magnetite surface interaction.

3.2. Investigation of the Surface Complex. Figure 4 displays the FTIR spectra of magnetite nanoparticles before and after phosphatation, compared to that of hydrated $FePO_4$. The strong absorption band around 580 cm^{-1} is characteristic of Fe−O bands of magnetite.[50] The broad vibration band between 3600 and 3200 cm^{-1} is associated with the OH stretching vibrations of water molecules (physisorbed molecular water), while those at 1621 cm^{-1} are associated with their bending mode. After phosphatation, the decrease of the OH bands is consistent with a reaction of the phosphoric acid group with the surface hydroxyls of the magnetite nanoparticles.[25,49,50] A broad P−O stretching band between 900 and 1200 cm^{-1} appears with two main features at 1045 and 1090 cm^{-1} and a shoulder over 900−975 cm^{-1}.

A similar broad band in the range 900−1200 cm^{-1} was observed after phosphatation of hematite, goethite, maghemite, and titania.[5,13,20,25,51] For these authors, the presence of absorptions at 900 −1000 and around 1200−1250 cm^{-1} would be characteristic of P—OH and P═O stretching bands, respectively. P—O stretching bands encountered in PO_4^{3-} units are often identified in the range 990−1100 cm^{-1} at 1070−1080, 1045, 1024, and 998 cm^{-1} ($FePO_4 \cdot H_2O$ in Table 2).[5,25,52−55] Some results of IR spectroscopy on phosphonyl or phosphoric acids grafted at the surface of metal oxides are given in Table 2. It appears not easy to discriminate the different observed bands and to assign them to a given phosphonate complex, the different groups bound to P having a strong influence on the electronic density around P and therefore on the position of the bands. So, strong P—O bonds lead to a band shift toward higher frequencies.[56] Thus, large differences in bands position or number are observed owing to pH and adsorption density of phosphate-based molecules.[13,56−59] All the more detailed IR studies reported that, at low pH and high surface loading, a bridging protonated complex is favored while, when the pH increases, a mononuclear protonated complex and then a mononuclear nonprotonated complex are formed (Table 2).[13,51,54,55,59,60] The amount of these complexes depends on the surface coverage, and they may be present simultaneously at the surface. However, the degree of protonation would be more important at low pH.[13,51,54,59] It appears from these IR analyses that a protonated binuclear phosphate complex is the main species at low pH. To ascertain the formation of this complex in our conditions, the 900−1200 cm^{-1} range of IR spectra has been fitted with a linear background and with peaks with Gaussian profile. Four bands have been identified at 816 (very small), 962, 1032, and 1110 ± 5 cm^{-1}. Generally, the symmetry of the adsorption complex is based on the number of the ν_3 band splitting and/or the presence or absence of the ν_1 vibration and on the comparison with IR spectra of aqueous phosphate species at different pH (Table 2).[5,13,51,54,59]

(48) Shafi, K. V. P. M.; Ulman, A.; Dayl, A.; Yan, X.; Yang, N.; Estournès, C.; Fournès, L.; White, H.; Rafailovich, M. *Chem. Mater.* **2002**, *14*, 1778.
(49) Nooney, M. G.; Campbell, C.; Murrel, T. S.; Lin, X. F.; Hossner, L. R.; Chusuei, C. C.; Goodman, D. W. *Langmuir* **1998**, *14*, 2750.
(50) Taylor, I. J. J.; Todd, M.; Davies, M. J.; Borioni, E.; Sangregorio, C.; Sen, T. *J. Magn. Magn. Mater.* **2004**, *284*, 145.
(51) Tjedor-Tjedor, M. I.; Anderson, M. A. *Langmuir* **1990**, *6*, 602.
(52) Feng, B.; Chen, J. Y.; Qi, S. K.; He, L.; Zhao, J. Z.; Zhang, X. D. *Biomaterials* **2002**, *23*, 173.
(53) Ait Salah, A.; Jozwiak, P.; Zaghib, K.; Garbarczyk, J.; Gendron, F.; Mauger, A. Julien C. M. *Spectrochim. Acta, Part A: Molec. Biomolec. Spectrosc.* **2006**, *65*, 1007.
(54) Persson, P.; Nilsson, N.; Sjöberg, S. *J. Colloid Interface Sci.* **1996**, *177*, 263.
(55) Zaghib, K.; Julien, C. M. *J. Power Sources* **2005**, *142*, 279.
(56) Sudarsan, V.; Muthe, K. P.; Vyas, J. C.; Kulshreshtha, S. K. *J. Alloys Compd.* **2002**, *336*, 119.
(57) Barja, B. C.; Tjedor-Tjedor, M. I.; Anderson, M. A. *Langmuir* **1999**, *15*, 2316.
(58) Sudakar, C.; Subbana, G. N.; Kutty, T. R. N. *J. Phys. Chem. Solids* **2003**, *64*, 2337.
(59) Elzinga, E. J.; Sparks, D. L. *J. Colloid Interface Sci.* **2007**, *308*, 53.
(60) Kowon, K. D.; Kubicki, J. D. *Langmuir* **2004**, *20*, 9249.

Table 2. Infrared Results Reported on Adsorption of Phosphate or Organophosphorus Molecules at the Surface of Metal Oxides

experimental conditions	phosphate complex	frequencies (cm^{-1})
phosphate adsorption on goethite, ATR-IR [13]	at low pH : $(FeO)_2PO_2$	952, 1047, 1092
	+ $(FeO)_2(OH)PO$	933, 1012, 1122
	at high pH only $(FeO)_2(OH)PO$	
phosphate adsorption on goethite, DRIFT[54]	at pH=3 $(FeO)(OH)_2PO$	1178 (ν(P═O)), 1001 (ν (P—OH)), 876 (ν (P—OH))
	intermediate	1122, 1049, 939
	at high pH:$FeOPO_3$	966. 1057
methylphosphonic acid adsorption on goethite, CIR-FITR[57]	$FeO(PO)OH(CH_3)^{x-1}$	1108 (ν (P═O)), 992 (ν (P—OFe)), 974 (ν (P—OH))
	$(FeO)_2PO(CH_3)^{2(x-1)}$ at pH=3.5 to 8	1095 (ν (P═O)), 1011 (ν (P—OFe)), 983 (ν (P—OFe))
phosphate at the surface of maghemite [20]	mono- and binuclear complexes	broadband centered at 1060
diphenyl phosphonic acid on titania, DRIFT[25]	binuclear phosphonate complex	998, 1024, 1045, 1070
commercial $FePO_4.2H_2O$		broad band at 1050
synthesized $FePO_4{\cdot}2H_2O$[53,55]		990, 1023, 1048, 1085
phosphate and phenyl phosphonic acid adsorption on ZrO_2 and TiO_2 membranes, FTIR[15]	trinuclear bonding mode with zirconia surface	disappearance of 940 (ν (P—OH)), 1220 (ν (P═O)) after grafting
phosphate adsorption on hematite, ATR-FITR[59]	at low pH:binuclear complex	964, 1007, 1117
	intermediate $(FeO)(OH)PO_2$	936, 1030, 1075
	at high pH:$FeOPO_3$	960, 1040, 1085
CIR-FITR analysis (in solution)[51]	**$(FeO)_2(OH)PO$** (main species) or $(FeO)(OH)_2PO$	1123 (P═O), 1006(P—O—Fe), 982 (P—OFe or P—OH)
orthophosphate/goethite surface complexes	$(FeO)_2PO_2$ or $(FeO)(OH)PO_2$	1044 (P—O), 1096(P—O)
	$FeOPO_3$	1001(P—O), 1025(P—O/P—O—Fe)
	H_3PO_4	890 (P—OH), 1006 (P—OH), 1174 (P═O)
	$H_2PO_4^-$	874 (P—OH), 940 (P—OH), 1075 (P—O), 1155 (P—O)
	HPO_4^{2-}	847 (P—OH), 989 (P—O), 1077 (P—O)
	PO_4^{3-}	1006 (P—O)
ATR-IR on H_3PO_4 at pH = 1.9	$H_3PO_4/H_2PO_4^-$ C_{3v}	1003, 1072, 1175
ATR-IR on H_3PO_4 at pH = 3.7	$H_2PO_4^-$ C_{2v}	937, 1076, 1153
ATR-IR on H_3PO_4 at pH = 7.6	HPO_4^{2-} C_{3v}	989, 1076
ATR-IR on H_3PO_4 at pH = 12.7	PO_4^{3-} *Th*	1001

Attenuated total refletance (ATR) experiments have been performed on H_3PO_4 solutions at different pH values, and our results given in Table 2 with the symmetry of each species are in good agreement with those of Tjedor-Tjedor and Anderson,[51] Elzinga and Sparks,[59] Arai and Sparks,[5] and Persson and al.[54] The triply degenerated symmetric stretching ν_3 is observed at 1110, 1032, and 962 cm^{-1} with the nondegenerate symmetric stretching ν_1 at 816 cm^{-1}, indicating a C_{2v} or a lower symmetry of the phosphate complex at the surface of magnetite. This symmetry is in agreement with that of the aqueous phosphate species at the pH of phosphatation ($H_2PO_4^-$ at pH = 3). Considering that the surface complex is protonated at this pH, the possible complexes are $(FeO)_2(PO)(OH)$, $(FeO)_2P(OH)_2$, and $(FeO)(PO)(OH)_2$. The $(FeO)(PO)(OH)_2$ complex should give IR spectra in which an absorption band assigned to the P═O mode appears at much higher frequency than the others, due to the concurrent presence in the structure of P═O and of two OH groups,[51] as observed in Table 2 and encountered in the spectrum of H_3PO_4 (P═O at 1175 cm^{-1}). The band at 1110 cm^{-1} leads to the advance that the main surface complex is not $(FeO)(PO)(OH)_2$ and is of binuclear type. The large intensity of the bands at high wavelengths assigned generally to P═O and Fe—O—P bonds, which is supported by the comparison of IR spectra of phosphated magnetite and commercial $FePO_4{\cdot}4H_2O$, is in favor of the $(FeO)_2(PO)(OH)$ complex. Moreover, our IR frequencies are in the same range of IR frequencies calculated by Kowon and Kubicki[60] for a monoprotonated binuclear complex: 879, 950, 989, 1032, 1113 cm^{-1}. Therefor, these IR interpretations and the fact that $H_2PO_4^-$ is the main species in our experimental conditions are in favor of a monoprotonated binuclear phosphate complex as described in Figure 5.

To further analyze the surface properties, the XPS analysis was carried out. Fe 2p XPS spectra of magnetite before and after phosphatation and those of the commercial $FePO_4{\cdot}4H_2O$ and FeO have been compared (Figure 6d). The Fe^{3+} and Fe^{2+} ions are distinguishable by XPS. Indeed, when Fe^{2+} ions are present at the surface, the satellite of the $2p_{3/2}$ peak around 719 eV characteristic of the Fe^{3+} ions in γ-Fe_2O_3 becomes less resolved due to the main $2p_{3/2}$ and $2p_{1/2}$ peaks broadening and to rising intensity at about 716 eV of the satellite for the Fe^{2+} ions.[5,49−51,61−64] The presence of Fe^{2+} at the probed surface of the magnetite is shown by the quiet absence of the satellite around 719 eV between the main Fe 2p peaks and by the comparison with Fe 2p peaks of commercial FeO containing only Fe^{2+} and commercial $FePO_4{\cdot}4H_2O$ containing only Fe^{3+}. Moreover, the Fe $2p_{3/2}$ peak position is around 710.6 eV for FeO (Fe^{2+}) and 712.3 eV for $FePO_4{\cdot}4H_2O$

(61) Aronniemi, J. P.; Sainio, J.; Lahtinen, J. *Surf. Sci.* **2005**, *578*, 108.
(62) Jung Chu, W. *Magn. Reson. Imag.* **1995**, *13*, 675.
(63) Fujii, T.; de Groot, F. M. F.; Sawatzky, G. A.; Voogt, F. C.; Hibma, T.; Okada, K. *Phys. Rev. B* **1999**, *59*, 3195.
(64) Kendelewicz, T.; Liu, P.; Doyle, C. S.; Brown, G. E., Jr; Nelson, E. J.; Chambers S. A. *Surf. Sci.* **2000**, *453*, 32.

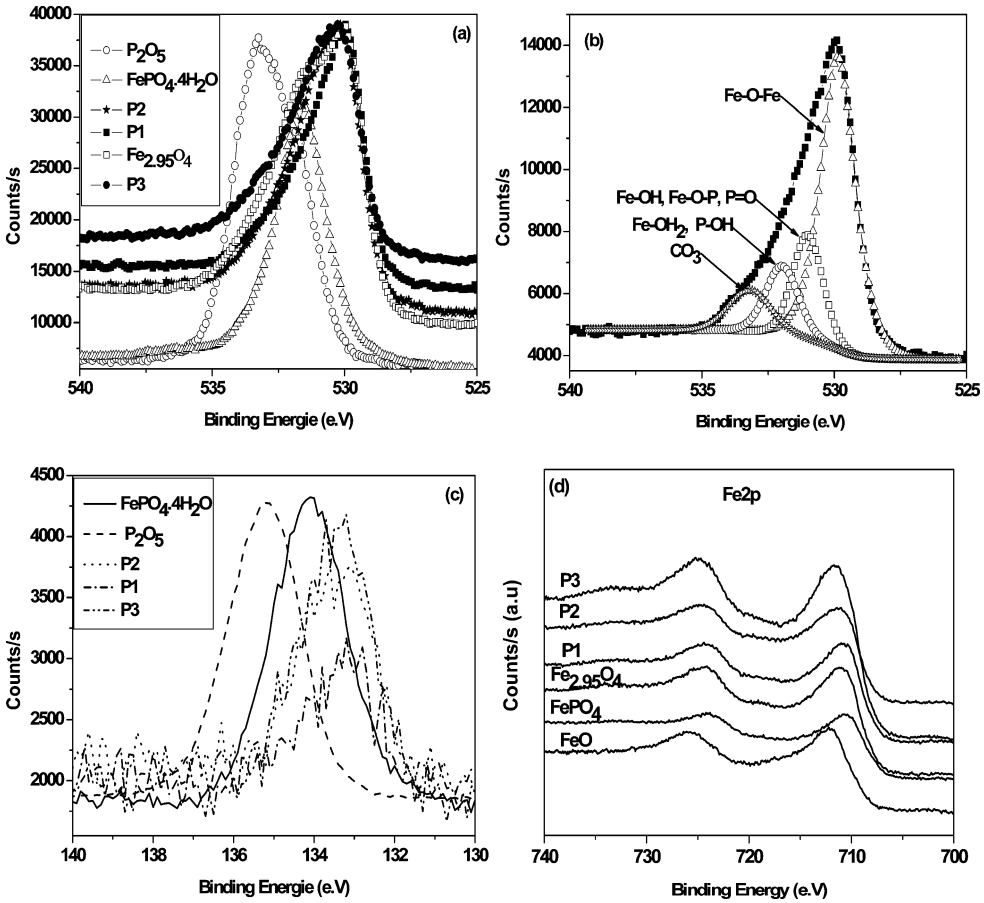

Figure 6. O1s peak in the XPS spectra of samples (a), deconvolution of the O1s peak of P1 sample (b), P2p peaks of samples (c), and Fe2p peaks of samples (d).

(Fe^{3+}), and its value is intermediate for magnetite: 711 eV. After phosphatation, the Fe2p bands in phosphated magnetite are very similar to those of magnetite (the Fe $2p_{3/2}$ peak positions respectively are 710.8, 711.0, and 711.3 eV for the P1, P2, and P3 samples), showing that some Fe^{2+} are still present at the probed surface of phosphated magnetite but suggesting that the amount of Fe^{3+} ions increases with the phosphatation rate.

The P2p signal showed a comparatively poor signal-to-noise ratio (Figure 6c). Moreover, the P2p signal is a doublet with $2p_{1/2}$ and $2p_{3/2}$ components. Their low theoretical energy separation (0.9 eV) means that the P2p signal is often assumed to be constituted of one peak and was fitted with a single peak. The XPS binding energies in phosphated magnetite as well as some values obtained in this study on commercial P_2O_5 and $FePO_4$ are given in Table 3 (Figure 6c). The binding energies of these last compounds are in good agreement with those reported by other authors.[65,66] The binding energy of phosphorus (133.6 eV whatever the phosphatation rate) in phosphated magnetite is in agreement with values reported by Nooney et al.[46] for the phosphatation of hematite and is lower than that of P in P_2O_5 and hydrated $FePO_4$, showing that the electron density around P atoms is higher in phosphated magnetite.

The consideration of O1s peaks may help to discriminate between the types of complex formed at the surface. Figure 6 displays the typical XPS spectrum of the O1s region, and the results are given in Table 3. The oxygen 1s peak of magnetite was deconvoluted into four spectral bands at 530.1, 531.0, 532.1, and 533.7 eV attributed respectively to the lattice oxygen (O^{2-}) in the metal oxide, to hydroxides, to water, and to carbonates at the surface of magnetite. After phosphatation, the O1s band is more complicated to analyze as there is now the contribution of P—O bonds. The binding energies of M—O—P and P═O species, reported in literature, occur in the range 531.3−532.1 eV and that of P—OH species occur in the range 532.6−533.6 eV.[32−34,67−69] These binding energies are consistent with those obtained in our characterization conditions for the commercial products: P_2O_5 and $FePO_4 \cdot 4H_2O$ (Table 3). Thus in our experimental conditions, the binding energy at 531.5 eV is attributed to P═O bonds[35,68] and to Fe—O—P bonds. Thus, the O1s peak of phosphated magnetite has been fitted with four peaks: 530.0 eV attributed to O—Fe; 531.5 eV to P═O, P—O—Fe, and Fe—OH; 532.6 eV to P—OH and H_2O; and 533.7 eV to carbonates. The XPS data are given in Table 3. The XPS results of phosphated magnetite samples have been compared

(65) Gaskell, K. J.; Smith, M. M.; Sherwood, P. M. A. *J. Vac. Sci. Technol. A* **2004**, *22*, 1331.
(66) Salim, M. A.; Khattak, G. D.; Fodor, P. S.; Wenger, L. E. *J. Non-Cryst. Solids* **2001**, *289*, 185.
(67) Adden, N.; Gamble, L. J.; Castner, D. G.; Hoffmann, A.; Gross, G.; Menzel, H. *Langmuir* **2006**, *22*, 8197.
(68) Adolphi, B.; Jähne, E.; Busch, G.; Cai, X. *Anal. Bioanal. Chem.* **2004**, *379*, 646.
(69) Zorn, G.; Gotman, I.; Gutmanas, E. Y.; Adadi, R.; Salitra, G.; Sukenik, C. N. *Chem. Mater.* **2005**, *17*, 4218.

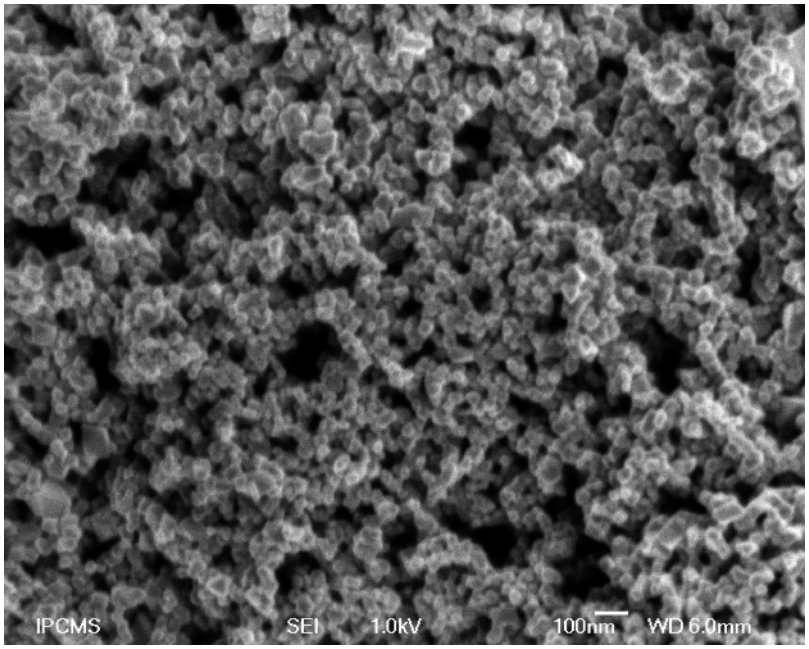

Figure 7. SEM micrograph of phosphated nanoparticles.

Table 3. XPS Results

		O1s				P2p
Fe_3O_4	P/Fe (atom %)	Fe—O—Fe	Fe—OH	Fe—OH_2	CO_3	
binding energy (eV)		530.1	531.0	532.1	533.7	
fwhm		1.7	1.6	1.8	2.1	
relative area without Fe—O contribution			0.43	0.39	0.18	
		Fe—O—Fe	Fe—O—P, P═O, Fe—OH	P—OH, Fe—OH_2	CO_3	P—O, P—OH, P═O
Fe_3O_4 P1	9.9	530.2	531.5	532.6	533.7	133.6
fwhm		1.7	1.6	1.8	2.1	
relative area without Fe—O contribution			0.56	0.25	0.19	
Fe_3O_4 P2	13.7	530.0	531.1	532.1	533.3	133.6
fwhm		1.7	1.6	1.8	2.1	
relative area without F—O contribution			0.55	0.26	0.18	
Fe_3O_4 P3	18.5	530.0	531.2	532.4	533.6	133.6
fwhm		1.7	1.6	1.8	2.1	
relative area without Fe—O contribution			0.51	0.29	0.20	
$FePO_4 \cdot 4H_2O$			531.5			134.1
P_2O_5	P—O—P = 533.2		531.5			135.1

with that of magnetite. The contribution of surface species has been emphasized by considering the relative area without Fe—O—Fe contribution. The relative area of the peak corresponding to OH in magnetite and to Fe—OH, P═O, and P—O—Fe in phosphated magnetite increases after phosphatation. Thus assuming a ligand exchange with surface OH groups to form the P—O—Fe link, that means that the contribution of a Fe—OH bond is replaced by the contribution of a Fe—O—P bond and a P═O bond. Therefore, the peak intensity is supposed to increase. Thus, the increase of the intensity of this peak supports the presence of P═O bonds. The area of the peak attributed to P—OH and H_2O in phosphated magnetite decreases after phosphation. No direct conclusion can be drawn because the intensity of this peak depends also on the hydration degree of phosphated magnetite which may vary due to the phosphatation. Two binuclear complexes were discussed in the IR analysis, one diprotonated or one with P═O and P—OH bonds; the observed decrease is nevertheless not consistent with a complex with two P—OH bonds. Thus, this result would confirm the monoprotonated complex designed from IR analysis.

3.3. Effect of Phosphatation on the Properties of Magnetite. Structural studies on phosphated magnetites were performed on three phosphated magnetite samples with phosphatation rates 2.06 (named P1), 3.9 (named P2), and 5.2 P-mg/g (named P3). SEM (Figure 7) and TEM measurements and X-ray diffraction patterns show that phosphatation does not modify the morphology and the crystallographic structure. The particle size remains constant with an average value around 39 nm. An EDX analysis on powders confirms that phosphorus-based species are present. The XRD pattern recorded after phosphatation exhibits the classical magnetite spinel structure. After phosphatation, the calculated lattice parameter a is 0.8393 ± 0.0005 and 0.8393 ± 0.0005 nm for P1 and P3 samples, respectively, equal to the lattice

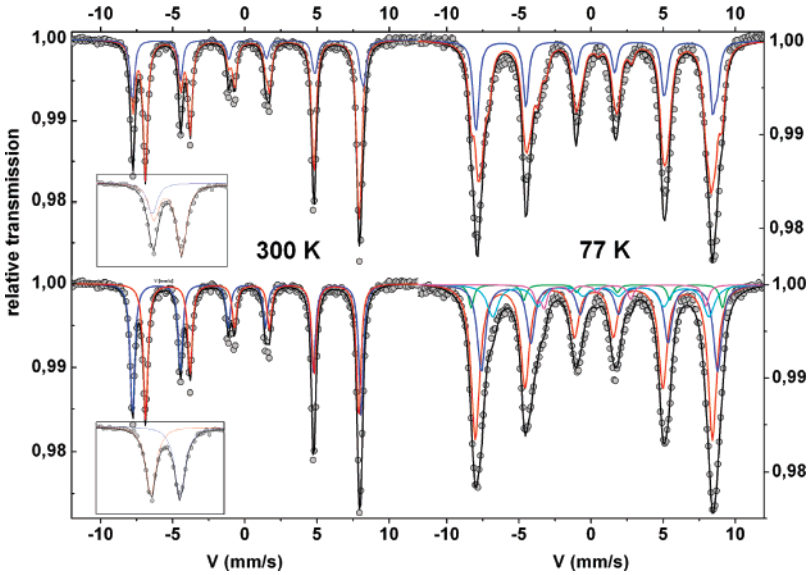

Figure 8. Mössbauer spectra at 300 K (left) and at 77 K (right) of the P3 sample. The bottom spectra show the decomposition into several components as generally done with a magnetite phase, while the top spectra were modeled assuming two stoichiometric phases as maghemite and magnetite (see text). The inset shows clearly the differences of the left outermost lines and the hyperfine spectra well-established for these two phases.

Table 4. ^{57}Fe Mössbauer Parameters for Magnetite (NP) and Phosphated Magnetite (P) Recorded at 300 and 77 K Refined on the Basis of the Two Fitting Procedures as Described in the Text[a]

		δ (mm/s) ±.01			2ε (mm/s) ±.01			B_{hf} (T) ±.1			% ±.5		
		NP	P3	P2	NP	P3	P2	NP	P3	P2	NP	P3	P2
300 K	Fe^{3+} T	0.32	0.31	0.29	0.00	0.01	0.01	49.1	50.4	48.9	45.0	49.5	48.9
	$Fe^{2.5+}$ O	0.66	0.67	0.66	0.04	0.02	0.01	45.7	46.9	45.6	55.0	50.5	51.1
77 K	Fe^{3+} T	0.40	0.36	0.39	0.00	0*	0*	50.7	50.8	50.4	42.0	50.9	42.0
	Fe^{3+} O1	0.54	0.56	0.54	-0.04	0*	0*	52.8	53.8	52.5	13.8	4.5	17.4
	Fe^{x+}O2	0.78	0.76	0.80	-0.03	0*	0*	49.9	50.6	49.6	25.1	26.3	19.5
	Fe^{y+}O1	0.86	0.84	1.00	0.02	0*	0*	46.0	46.3	45.5	15.1	12.5	16.3
	Fe^{2+}O2	1.15	1.08	1.25	2.19	2.29	2.10	34.5	34.5	34.8	4.0	4.9	4.8
300 K	γ-Fe_2O_3T	0.29	0.30	0.30	0*	0*	0*	49.4	49.3	48.8	9.2	9.3	8.6
	O	0.40	0.40	0.40	0*	0*	0*	49.6	50.0	49.7	15.5	15.7	14.2
	Fe_3O_4 T	0.31	0.31	0.30	0*	0*	0*	48.7	46.0	45.6	25.2	25.0	25.6
	O	0.66	0.66	0.66	0*	0*	0*	45.7	49.1	48.8	50.1	50.0	51.6

[a] O = octahedral position, T = tetrahedral position, x, y = intermediate valence state, $2 < x, y < 3$.[73] δ: isomer shift, Γ: width at half-height, 2ε: quadrupole shift, B_{hf}: hyperfine field, %: amount of the iron cations on the different sites. * These values were fixed during the fitting procedure.

parameter before phosphatation (0.8395 ± 0.0005 nm). These values are very close to that of stoichiometric magnetite and far from that of maghemite (0.8346 nm, JCPDS file 39-1346), indicating that a slight amount of Fe^{2+} has been oxidized.

Mössbauer spectrometry is a priori the most adapted method to evaluate the exact deviation from stoichiometry δ in $Fe_{3-\delta}O_4$.[39] The Mössbauer spectra of phosphated magnetite before and after phosphatation (P2, P3) at 300 K and 77 K are quite similar: only one example is illustrated in Figure 8. At 300 K, one distinguishes clearly two resolved sextets (see Figure 8 left bottom), one attributed to Fe^{3+} in the A site of spinel magnetite (the outer sextet) and one attributed to $Fe^{2.5+}$ in the B site, while the Mössbauer spectrum at 77 K displays a sextet with broadened and symmetrical lines (see Figure 8 right bottom), as expected.[70] The values of hyperfine parameters before and after phosphatation are listed in Table 4 and are consistent with those generally reported for magnetite, except for the sextet area leading to a ratio $Fe_{tetra}^{3+}/Fe_{octa}^{3+,2+}$ of about 1, which strongly differs from the expected value equal to 0.50; in addition,

(70) Doriguetto, A. C.; Fernandes, N. G.; Persiano, A. I. C.; Nunes Filho, E.; Grenèche, J. M.; Fabris, J. D. *Phys. Chem. Minerals* **2003**, *30*, 249.

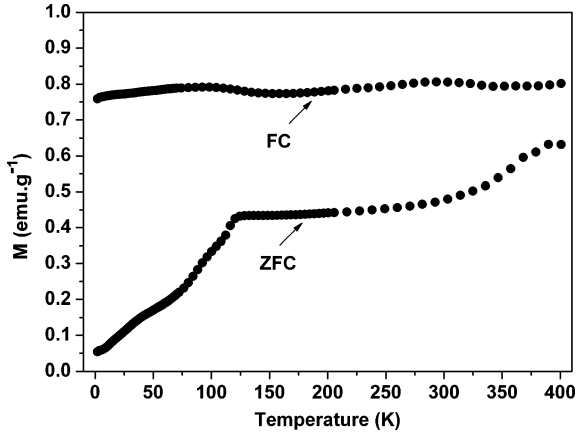

Figure 9. ZFC/FC curves of phosphated magnetite nanoparticles (P3) under a field of 10 Oe.

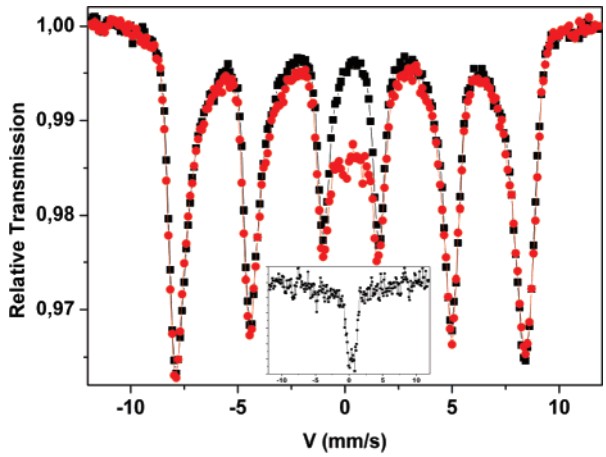

Figure 10. Comparison of Mössbauer spectra at 77 K of magnetite with an average grain size of 12 nm before (in black) and after phosphatation (in red). The inset shows the spectrum resulting from the difference between the two previous spectra, giving clear evidence for a quadrupolar doublet.

the content of Fe^{2+} at 77 K is estimated at about 5% which is lower than the expected value of 10%.[71−73] The intensity ratio of sextet A to sextet B is very sensitive to the stoichiometry of magnetite.[72−75] The deviation from 0.50 is generally attributed to a superstoichiometry in oxygen or cationic vacancies; there would be oxidation of Fe^{2+} on the B site in Fe^{3+} accompanied by vacancies of formation, giving the general formula: $Fe^{3+}{}_A[Fe^{2.5+}{}_{2-6\delta}Fe^{3+}{}_{5\delta}\square_\delta]_BO_4{}^{2-}$. Calculations of the stoichiometry deviation from the relative subspectral area with the formula reported by Voogt et al.[76] and with that of Paramês et al.[77] give for both adsorptions a similar deviation $\delta = 0.08$ in $Fe_{3-\delta}O_4$, leading thus to a general formula of $Fe_{2.92}O_4$. The values of isomer shift lead

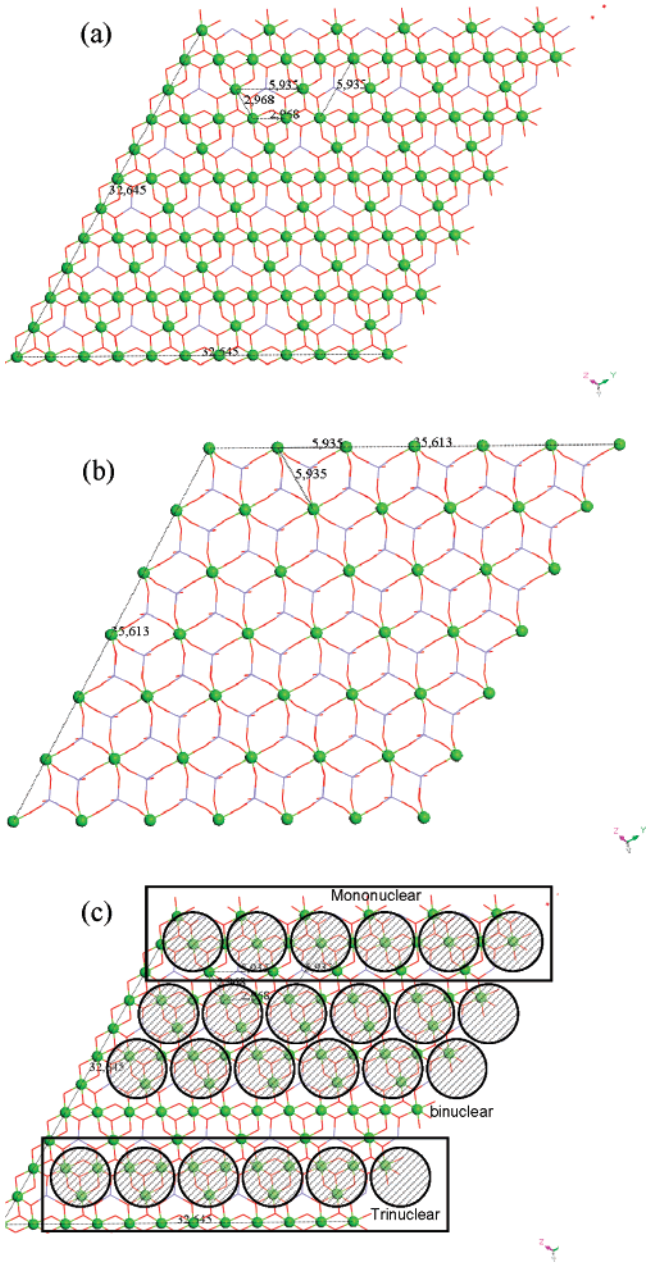

Figure 11. (111) plane of magnetite containing Oh sites with a high (a) or a low (b) density and occupancy of a phosphate molecule as a function of the type of complex (mono-, bi-, or trinuclear) in the denser Oh plane (c).

to an estimate of the Fe valence state and, then, to composition. Assuming the isomer shift of $Fe_{tetra}{}^{3+}$, $Fe_{octa}{}^{3+}$, and $Fe_{octa}{}^{2+}$ at 0.25, 0.40, and 1.00 at 300 K, and 0.40, 0.54, and 1.15 at 77 K, respectively, one obtains $Fe_{2.89}O_4$. From these results, it may be concluded that the phosphated nanoparticles are magnetite with a deviation from stoichiometry leading to a mean $Fe_{2.90\pm0.02}O_4$ composition. Thus, an oxidation of Fe^{2+} has occurred during the phosphatation step. However, as already observed with unphosphated magnetite nanoparticles, this deviation from stoechiometry may originate from the surface of nanoparticles, the core remaining stoichiometric.[39] First, the comparison of the spectra at 77 K with those obtained with γ-Fe_2O_3−Fe_3O_4

(71) Khollam, Y. B.; Dhage, S. R.; Potdar, H. S.; Deshpande, S. B.; Bakare, P. P.; Kulkarni, S. D.; Date S. K. *Mater. Lett.* **2001**, *56*, 571.
(72) Kendelewicz, T.; Liu, P.; Doyle, C. S.; Brown, G. E., Jr; Nelson, E. J.; Chambers S. A. *Surf. Sci.* **2000**, *453*, 32.
(73) Visalakshi, G.; Venkataswaran, G.; Kulshreshtha, S. K.; Moorthy, P. N. *Mater. Res. Bull.* **1993**, *28*, 829.
(74) Balasubramaniam, C. ; Khollam, Y. B.; Banerjee, I.; Bakare, P. P.; Date, S. K.; Das, A. K.; Bhoraskar, S. V. *Mater. Lett.* **2004**, *58*, 3958.
(75) Simmons, G. W.; Leidheiser, H. Jr. *Application of Mössbauer Spectroscopy*; Cohen, R. L., Ed.; Academic Press: New York, 1976; Vol. 1, p 106.
(76) Voogt, F. C.; Fuji, T.; Smulders, P. J. M., Nielsen, L.; James, M. A.; Hibma, T. *Phys. Rev. B* **1999**, *60*, 11193.
(77) Paramês, M. L.; Mariano, J.; Rogalski, M. S.; Popovici, N.; Conde, O. *Mater. Sci. Eng. B* **2005**, *118*, 246.

solid solutions with similar stoechiometry deviation shows that the phosphated magnetite is not such a solid solution.[78] Second, another way to verify this hypothesis is the consideration of ZFC/FC curves. The temperature dependence of the ZFC and FC magnetization give information on the stoechiometry of magnetite since the Verwey transition temperature (T_V) is very sensitive to deviation from stoechiometry.[39,79] Indeed T_V is reported to decrease from 125 to 100 K from $Fe_{2.995}O_4$ to $Fe_{2.934}O_4$. The ZFC curve of phosphated magnetite is presented in Figure 9 and displays, as for magnetite, two transition temperatures: one around 120 K corresponding to the Verwey transition temperature (T_V) of pure magnetite and the other at about 50 K, attributed to the relaxation process, usually observed in monocrystalline stoichiometric magnetite.[80] The value of T_V is similar to that reported for bulk magnetite.[81] The value of T_V at 120 K and Mössbauer results confirm that only the surface of phosphated nanoparticules presents a deviation from stoichiometry and that the main volume is constituted of stoichiometric magnetite. Such a description of phosphated nanoparticles would explain also the difference in stoichiometry deviation calculated from lattice parameter and from Mössbauer spectra and is consistent with results of Perriat et al. on the oxidation of titanomagnetite spinels.[82,83] Consequently, a second fitting procedure involving two phases, i.e., stoichiometric magnetite and stoichiometric maghemite, was successfully obtained at 300 K as illustrated in Figure 8 (left top). The theoretical tetrahedral and octahedral Fe ratios are assumed in each of these phases (0.33 and 0.375, respectively, for tetrahedral sites) as one can observe particularly for magnetite in the upper inset of Figure 8. It is found that the hyperfine structure can be decomposed into about 25% maghemite and 75% magnetite, assuming the same value of recoil-free factor. Assuming a core−shell (magnetite−maghemite) description for such nanoparticules of 40 nm diameter, the thickness of the maghemite shell is 1.8 nm, corresponding thus to about three elementary cells. Such an approach which can be also a priori applied at 77 K remains less reasonable, because of the rather complex hyperfine structure of magnetite. One example of modeling is illustrated in Figure 8 (right top) considering the same proportions as found at 300 K; it is important to emphasize that this modeling at 77 K does not allow the proportions of both phases to be accurately estimated.

Mössbauer spectrometry may also allow one to distinguish and to identify the iron ions involved in phosphate complexes. Mössbauer analyses (at 77 K) of phosphated magnetite with smaller grain size (12 nm), for which the contribution of surface species are no more negligible, are reported in Figure 10. A supplementary quadrupolar doublet is clearly observed at the center (see the inset of Figure 10), similar to that reported by Tronc et al. for phosphated maghemite and attributed to surface iron−phosphate complexes.[20] The isomer shift value of this quadrupolar doublet indicates that phosphatation occurs with Fe^{3+} ions in octahedral sites.

This result is in agreement with studies on the atom termination of the (111) Fe_3O_4 surface plane (which is the main surface plane of 40 nm magnetite nanoparticles) which have established that the top atom layer is made of ferrous ions that originate from the octahedral (Oh) interstitial sites.[84−86] Indeed, along the (111) direction, magnetite may be described by a stacking of layers of iron in Oh or Td sites and oxygen, schematically represented by $Fe_{tet1}-O_1-Fe_{oct1}-O_2-Fe_{tet2}-Fe_{oct2}-Fe_{tet1}-O_1$. There are thus two types of planes containing Oh sites along the (111) direction, given in Figure 11. It must be noted that there are still investigations to discriminate which plane is the top layer. One plane involves dense packing of Oh sites with 9.8 Fe atom/nm^2 (Fe_{oct1}) (Figure 11a). The other plane is less dense with 3.2 Fe atom/nm^2 (Fe_{oct2}) (Figure 11b). In the latter plane, the distances between iron atoms is 5.96 Å, and as the surface of the phosphate molecule is 24 Å^2, which gives a circular area with a radius of 2.76 Å, the grafting in this plane can only be of mononuclear type. However, the consideration of a maghemite ($(Fe^{3+})_A(Fe^{3+}_{3/5}\square_{1/5})_BO_4$) layer at the surface of magnetite ($(Fe^{3+})_A(Fe^{3+}Fe^{2+})_BO_4$) nanoparticles, which displays the same structure as magnetite but with vacancies on Oh sites, means that 1/6 of Oh sites are not occupied. Thus from such a crystallographic point of view, the grafting on the less dense Oh plane (3.2 Fe/nm^2 for magnetite and 2.7 sites/nm^2 for maghemite) appears no more possible.

In the other plane (9.8 Fe atom/nm^2 for magnetite and 8.2 sites/nm^2 for maghemite), due to the area of the phosphate molecule and to the distances between atoms, a monodendate grafting "allows" only one site among three sites to be grafted, that means that 3.3 sites/nm^2 and a binuclear one "occupy" also three sites, i.e., 3.3 sites/nm^2. Thus in monodentate or bidentate grafting, the Fe sites are not all involved, which make the presence of vacancies negligible. Nevertheless, it is not the case with a tridentate grafting which "needs" all the iron sites (9.9 sites/nm^2). From this crystallographic consideration, the top atom layer of magnetite-based nanoparticles is made up of the denser plane containing Oh sites.

Conclusion

The study of the phosphatation of magnetite nanoparticles has demonstrated that magnetite nanoparticles exhibit interesting adsorbent properties by comparison with the more commonly used iron hydroxides: the goethite. Characterization of phosphated magnetite has demonstrated that phos-

(78) Schmidbauer, E.; Keller, M. *J. Magn. Magn. Mater.* **2006**, *297*, 107.
(79) Guigue-Millot, N.; Keller, N.; Perriat, P. *Phys. Rev. B* **2001**, *64*, 012402.
(80) Skumryev, V.; Blythe, H. J.; Cullen, J. Coey, J. M. D. *J. Magn. Magn. Mater.* **1999**, *196−197*, 515.
(81) Aragon, R.; Shepherd, J. P.; Koenitzer, J. W.; Buttrey, D. J.; Rasmussen, R. J.; Honig, J. M. *J. Appl. Phys.* **1985**, *57*, 3221.
(82) Guigue-Millot, N.; Champion, Y.; Hytch, M. J.; Bernard, F.; Bégin-Colin, S.; Perriat, P. *J. Phys. Chem. B* **2001**, *105*, 7125.
(83) Domenichini, D.; Perriat, P.; Merle, J.; Basset, K.; Guigue-Millot, N.; Bourgeois, S. *J. Mater. Chem.* **1999**, *9*, 1179.
(84) Ahjoudj, J.; Martinsky, C.; Minot, C.; Van, Hove, M. A.; Somorjai, G. A. *Surf. Sci.* **1999**, *443*, 133.
(85) Lovely, G. R.; Brown, A. P.; Brydson, R.; Kirkland, A. I.; Meyer, R. R.; Chang, L. Y.; Jefferson, D. A.; Falke, M.; Bleloch, A. *Micron* **2006**, *37*, 389.
(86) Zhu, L.; Yao, K. L.; Liu, Z. L. *Phys. Rev. B* **2006**, *74*, 035409(10).

phatation occurs by interaction with Fe^{3+} in octahedral sites with formation of monoprotonated binuclear species. The presence of binuclear species and crystallographic considerations imply that the top layer is made up of the (111) denser plane containing Oh sites.

Acknowledgment. The authors wish to thank Cedric Leuvrey, Corinne Ulhaq-Bouillet, and Pierre Rabu for their assistance with the SEM and TEM analysis and crystallographic studies.

CM071046V